Impacts of high precipitation on the energy and water budgets of a humid boreal forest

Pierre-Erik Isabelle [a,b], Daniel F. Nadeau [a,b,*], François Anctil [a,b], Alain N. Rousseau [d], Sylvain Jutras [a,c], Biljana Music [e]

[a] *CentrEau - Water Research Center, Université Laval, 1065 avenue de la Médecine, Québec, QC, Canada.*
[b] *Department of Civil and Water Engineering, Université Laval, 1065 avenue de la Médecine, Québec, QC, Canada.*
[c] *Department of Forestry and Wood Science, Université Laval, 2405 rue de la Terrasse, Québec, QC, Canada.*
[d] *Institut national de la recherche scientifique - Centre Eau Terre Environnement, 490 rue de la Couronne, Québec, QC, Canada.*
[e] *Ouranos Consortium, 550 Sherbrooke St West, Montréal, QC, Canada*

Abstract

The boreal forest will be strongly affected by climate change and in turn, these vast ecosystems may significantly impact global climatology and hydrology due to their exchanges of carbon and water with the atmosphere. It is now crucial to understand the intricate relationships between precipitation and evapotranspiration in these environments, particularly in less-studied locations characterized by a cold and humid climate. This study presents state-of-the-art measurements of energy and water budgets components over three years (2016-2018) at the Montmorency Forest, Québec, Canada: a balsam fir boreal forest that receives ~1600 mm of precipitation annually (continental subarctic climate; Köppen classification subtype Dfc). Precipitation, evapotranspiration and potential evapotranspiration at the site are compared with observations from thirteen experimental sites around the world. These intercomparison sites (89 study-years) encompass various types of climate and vegetation (black spruces, jack pines, etc.) encountered in boreal forests worldwide. The Montmorency Forest stands out by receiving the largest amount of precipitation. Across all sites, water availability seems to be the principal evapotranspiration constraint, as precipitation tends to be more influential than potential evapotranspiration and other factors. This leads to the Montmorency Forest generating the largest amount of evapotranspiration, on average ~550 mm y^{-1}. This value appears to be an ecosystem maximum for evapotranspiration, which may be explained either by a physiological limit or a limited energy availability due to the presence of cloud cover. The Montmorency Forest water budget evacuates the precipitation excess mostly by watershed discharges, at an average rate of ~1050 mm y^{-1}, with peaks during the spring freshet. This behaviour, typical of mountainous headwater basins, necessarily influence downstream hydrological regimes to a large extent. This study provides a much needed insight in the hydrological regimes of a humid boreal-forested mountainous watershed, a type of basin rarely studied with precise energy and water budgets before.

Keywords: Evapotranspiration; Energy Budget; Boreal Forest; Water Budget; Watershed Hydrology; Eddy-Covariance

---

Preprint submitted to Agricultural and Forest Meteorology *April 1, 2019*
*Corresponding author: *Email address:* daniel.nadeau@gci.ulaval.ca (Daniel F. Nadeau)

1. Introduction

The boreal forest covers roughly 14% of the Earth emerged surface, globally enclosing 30% of the world's forests (Brandt et al., 2013; Gauthier et al., 2015). It is the second largest vegetated area in extent (12 to 14 million km^2) behind tropical forests (Landsberg & Gower, 1997). Furthermore, it sequesters 20% of the global forest carbon (Pan et al., 2011). On the whole, the circumpolar boreal biome controls fluxes of carbon and water over a huge area and thus impacts the Earth's global climatology and hydrology. In return, global climate tremendously affects the boreal forest; this biome will in all likelihood experience one of the strongest warming in the future (IPCC, 2013), lengthening the growing season and forest productivity (Kauppi et al., 2014; Schaphoff et al., 2016; Liu et al., 2019). In some regions, these changes could be modulated by lower precipitation leading to conditions where evapotranspiration is unable to meet an increase in evaporative demand (Barber et al., 2000; Lloyd & Bunn, 2007; Walker et al., 2015). However, boreal forest regions of northeastern North America, enduring large precipitation, could be sheltered from such destructive effects (D'Orangeville et al., 2016).

For these reasons, there is a need to further our understanding of the intricate relationship between precipitation (P), evapotranspiration (E), and evaporative demand in various regions of the boreal forest. The first step towards this goal is to quantify the energy and water budgets of the ecosystem.

The surface energy budget of for a watershed covered by forest can be described as follows:

$$R_n = H + \lambda E + G + \Delta Q \tag{1}$$

where R_n is the net radiation; H, the sensible heat flux; λE, the latent heat flux associated with evaporation of surface water and transpiration of vegetation, or evapotranspiration; G, the soil heat flux; ΔQ, variations in storage of heat in the air and biomass below a certain height – all terms are expressed as energy fluxes per surface area in W m^{-2}.

Similarly, the water budget of a watershed can be described as:

$$P = E + O + \Delta S \tag{2}$$

where P is the total precipitation; E, the evapotranspiration; O, the watershed outflow, in streams and grounds; ΔS, the storage variations of water in the ground via water table and soil water content fluctuations and above the ground via snowpack accumulation – with all terms are expressed in mm; that is for a given time interval as water volumes per surface area of the watershed. In both budgets, the left-side terms are input of energy or water, while right-side terms generally express outputs. E is the obvious link between energy and water budgets, appearing in both Equations (1) and (2) (as a

mass flux in the former and as a water height in the second, the latter being the mass flux multiplied by the time interval over water density).

The boreal forest energy budget has been documented at length during the Boreal Ecosystem Atmosphere Study (BOREAS; Sellers et al., 1995; 1997) and in the ensuing measurement years at the Boreal Ecosystem Research and Monitoring Sites (BERMS; Barr et al., 2002). The mostly evergreen canopy absorbs a large amount of solar radiation year-long (Sellers et al., 1997). In the BERMS studied area, the absorbed energy returns to the atmosphere mostly by means of *H* (Saugier et al., 1997; Barr et al., 2001; Coursolle et al., 2006; Gao et al., 2017), except in the presence of deciduous species (Blanken et al., 1997; Zha et al., 2010; Brown et al., 2014). The incidentally low *E* rates still account for a large portion of annual *P*, leaving small volumes to generate watershed outflows (Nijssen & Lettenmaier, 2002; Barr et al., 2012). Similar results were also observed in Scandinavia (Ilvesniemi et al., 2010) and Russia (Oltchev et al., 2002).

Because of their climate, the aforementioned BERMS sites cannot effectively describe the effects of high rainfall on the energy and water budgets of the boreal forest. While the humid forests of northeastern North America have been studied for their carbon budget (Giasson et al., 2006; Bergeron et al., 2007; Payeur-Poirier et al., 2012), a detailed description of the interrelationships between the energy and water budgets is still lacking. Besides, very few studies have used precise *E* measurements to assess the water balance of the boreal forest at the watershed scale (*e.g.*, Nijssen & Lettenmaier, 2002; Ilvesniemi et al., 2010; Barr et al., 2012), none in precipitation-heavy regions, to the best of our knowledge. Given that these regions are expected to undergo changing climate conditions, more studies are needed.

This work assesses the impacts of high precipitation on boreal forest energy and water budgets for the balsam fir – white birch bioclimatic domain. The experimental site is a small watershed featuring an extensive instrumental setup measuring most terms of the energy and water budgets. The watershed, at the southern extent of the circumpolar boreal biome, is subject to particularly high precipitation, making it an ideal site for this study. This paper is specifically interested in: (i) comparing the energy and vertical water budgets of the main study site and specifically *E*-*P* interactions with observed values in other boreal forest sites around the world; and (ii) quantify the impact of *E*-*P* interactions on the water budget, specifically on measured discharges. Results are based on three-year flux tower measurements in two locations featuring trees at different stages of maturity. Comparison data include 89 study-years spread over 13 sites around the circumpolar boreal biome.

2. Main Study Site

2.1. Site description

The main study site is located in the Montmorency Forest (47°17’18”N; 71°10’05.4”W), 80 km north of Québec City, Canada (BF1993 and BF2003 in Figure 1c), part of the balsam fir – white birch

bioclimatic domain. Specifically, two flux towers were installed in the "Bassin Expérimental du Ruisseau des Eaux-Volées" (BEREV) (Lavigne, 2007; Tremblay et al., 2008, 2009; Nöel et al., 2014; Isabelle et al., 2018a). This experimental watershed lies at a mean altitude of 750 m above mean sea level (AMSL) with peaks at 1000 m AMSL. Figure 1a presents the boundaries of two sub-catchments of the BEREV covering an area of 3.6 km^2. The sub-catchment A, located upstream of the sub-catchment B, is gauged and has a 1.2-km^2 area; the sub-catchment B, which is also gauged, has a 2.4-km^2 area. The general slope of the entire catchment, referred to here as AB, is 0.064 m m^{-1}.

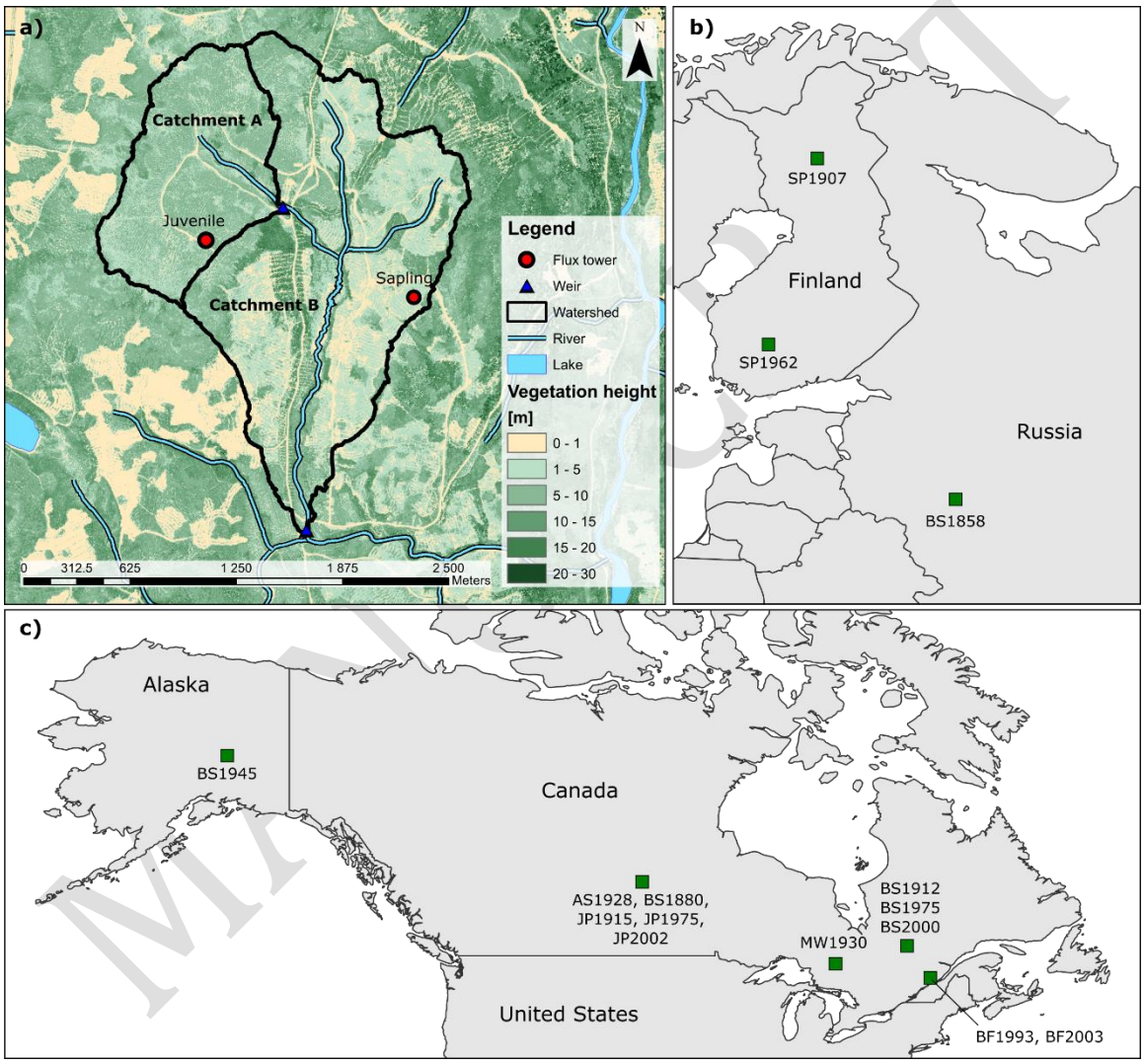

Figure 1: a) Location of instruments at the study site, with catchment boundaries and vegetation height from LiDAR surveys (Source: Ministère Forêts, Faune et Parcs du Québec); b) Location of European study sites; c) Location of study sites in North America.

The vegetation of both catchments consists mostly of balsam fir (*Abies balsamea* (L.) Mill) along white birch (*Betula papyrifera* Marsh) and white spruce (*Picea glauca* (Moench) Voss) (Lavigne, 2007; Tremblay et al., 2008, 2009). Trees reach heights between 4-8 m in the sub-catchment A, the product of natural regeneration after the logging of 85% of the trees in 1993. The trees are labeled as "juvenile", hence the flux tower name. Sub-catchment B was logged progressively between 2000 and 2010, but not entirely. Tree height distribution is heterogeneous, but in the vicinity of the flux tower prevails trees 2-4 m tall that was classified as "sapling", hence naming the flux tower.

The Montmorency Forest is under the influence of a continental subarctic climate (Köppen classification subtype Dfc) with a short and cool growing season and high volumes of year-round precipitation. Mean annual temperature is 0.5°C and mean annual precipitation amounts to 1583 mm (40% as snow) over the period of 1981-2010, as per Environment and Climate Change Canada (Station "Foret Montmorency", available at: http://climat.meteo.gc.ca/historical_data/search_historic_data_f.html).

2.2. Instrumental setup

Two flux towers were installed in the BEREV in October 2015: the Juvenile and Sapling flux towers (see Figure 1a). The Juvenile flux tower is a 15-m scaffolding structure featuring two sets of sonic anemometers and CO_2/H_2O gas analyzers (IRGASONs, Campbell Scientific, USA). The two devices are mounted 14.63 m above the ground, or ≈8 m above the top of the canopy, and face opposite directions (303°, northwest; and 118°, southeast). This feature allows for optimal flux quality control, since wind interference by the tower structure and devices is avoided by combining both time series based on wind direction. Both devices were installed parallel to the local 12° northeast-facing slope. This alignment is required to apply the eddy-covariance method on sloped terrain (Turnipseed et al., 2002; Hammerle et al., 2007; Hiller et al., 2008; Goulden et al., 2012; Nadeau et al., 2013b; Stiperski & Rotach, 2016), as it weakens flow distortion (Geissbühler et al., 2000; Oldroyd et al., 2016).

The Sapling flux tower is a 10-m triangular tower with one eddy-covariance system (IRGASON, Campbell Scientific, USA) mounted at a height of 8.5 m, or ≈5 m above the canopy. As the tower is located on a plateau, the instrument was leveled. Measurements from all eddy-covariance systems were sampled at 10 Hz and logged separately on three CR3000 dataloggers (Campbell Scientific, USA).

The Juvenile and Sapling towers also featured measurements of net radiation and soil heat flux. Net radiation was measured with 4-component radiometers (CNR4, Kipp and Zonen, The Netherlands). At the Juvenile tower, two devices were mounted at 15 and 10 m above the surface and parallel to 12° northeast-facing slope to follow the inclination of the eddy-covariance systems (Nadeau et al., 2013a; Serrano-Ortiz et al., 2016). At the Sapling tower, one device was installed 7 m above the ground and leveled.

The flux towers were also equipped with general meteorological measurements. Air temperature and relative humidity were measured with standard probes (HC2S3 and HMP45C,

Campbell Scientific, USA). The Juvenile tower included a profile of four probes installed at heights of 3.29, 5.68, 10.77 and 14.96 m above the ground. The Sapling tower featured one probe at 2.10 m. Wind speed and direction were measured using wind vanes (05103, RM Young, USA), namely, two of them were installed at the Juvenile tower at heights of 8.53 and 14.63 m above ground, while one was installed at 3 m above ground at the Sapling tower.

The Juvenile site also featured measurements of biomass temperature using a set of 39 thermistors (Omega Engineering, USA) placed in five trees around the flux tower (3 balsam firs, 1 white spruce and 1 white birch). Three thermistors were installed in each tree trunk (one in the center of the bole, one on the south side and one on the north side, both beneath the bark) at a height of 1.3 m. The temperature of the top portion of each tree trunk was also monitored with thermistors placed on the north and south sides beneath the bark at two-thirds of the tree height. 15 thermistors were installed in tree branches: either on the top of the lowest branches or on the bottom of the top branches, on the north and south sides of each monitored tree.

Total precipitation and complementary measurements of air temperature, relative humidity, and atmospheric pressure were measured at a station located ≈4 km north of the study sites and operated by the Québec government (MELCC, 2019). To obtain the most accurate snowfall measurements, the site also had a Double-Fence Intercomparison Reference (DFIR, Pierre et al., 2019), which is the reference to avoid solid precipitation under-catch (Yang, 2014). Data are available and substituted to the regular station between November 1 and March 31 each year for the part of our analysis that focuses on the Montmorency Forest watershed budget (see section 5.2). We did not use DFIR data for the comparison between boreal sites (section 5.1), as the precipitation of the other sites were not corrected for undercatch. Discrepancies in measurements with and without undercatch corrections at Montmorency Forest are discussed in section 5.2.

The setup also includes discharge measurements, as illustrated in Figure 1a. Discharge were obtained using v-notch weirs also operated by the Québec government (Station 51004 and 51007, available at: https://www.cehq.gouv.qc.ca/hydrometrie/historique_donnees/). Daily mean runoffs were used in this study.

2.3. Data processing

Eddy-covariance raw 10-Hz measurements were processed using EddyPro©, version 6.0 (LI-COR Biosciences, USA). The procedure included linear detrending, correction of low-pass (Moncrieff et al., 1997) and high-pass (Moncrieff et al., 2004) filtering effects, covariance maximization, density fluctuations compensation with the Webb correction (Webb et al., 1980). Coordinate rotation of wind speed was performed using a sector-wise planar fit (Wilczak et al., 2001), since this procedure is recommended for eddy-covariance measurements on slopes (Ono et al., 2008; Oldroyd et al., 2016). Spikes, amplitude resolution artifacts, unrealistic drop-outs, outliers and discontinuities, as well as other artifacts were detected and removed using the statistical tests of Vickers & Mahrt (1997).

Turbulent fluxes were computed using a 30-min averaging period. Errors associated with fluxes were quantified using the random uncertainty method of Finkelstein & Sims (2001).

Data runs during rainfall events were filtered out, because rain can obstruct the path of the open gas analyzer light signal. Periods when winds were blowing from a 90° sector centered on the back of the devices were also removed, as these conditions imply that the flow of air is distorted by the tower structure. Poor data quality was assessed and removed using the 0-1-2 criteria of Mauder & Foken (2011). Periods when turbulent fluxes largely violated the energy budget (*i.e.*, $H + \lambda E > 5R_n$) were discarded. Filtering was completed by a meticulous visual inspection to detect and remove periods of clear malfunction. This rigorous filtering procedure removed ≈35% and ≈50% of data segments for H and λE, respectively, for both sites between 2016 and 2018 inclusively.

For the Juvenile site, time series of fluxes from both eddy-covariance setup were combined using wind direction. To further complete these time series, the Juvenile and Sapling fluxes were gap-filled using marginal distribution sampling (MDS) as described in Reichstein et al. (2005) (see their Appendix A and Figure A1), as recommended by Moffat et al. (2007). This procedure left only ≈5% and ≈20% of missing data for H and λE, respectively. Remaining gaps were filled with monthly linear regression with zero-set origin between fluxes and net radiation.

As was the case for eddy-covariance data, all complementary meteorological and biomass temperature measurements were subjected to a rigorous filtering procedure that began with a careful visual inspection to detect clear periods of malfunction. Some meteorological variables received specific filtering procedures. Shortwave downwelling radiation was capped by maximum theoretical values calculated following Whiteman & Allwine (1986). For every temperature-humidity sensor, humidity values were capped using temperature-dependent maximum humidity.

For every variable, gap-filling was performed by merging time series from different devices with monthly linear regressions using a clear step-by-step procedure: (i) a variable is filled with other on-site devices by order of proximity; (ii) variable are next filled with the other site similar devices; and (iii) the few remaining gaps are completed with data from the nearby governmental station.

Soil heat fluxes were measured with soil heat flux plates, but energy storage above the plates (ΔQ_G [W m^{-2}]) were also calculated and included in G. They were obtained from the standard calorimetric method (Ochsner et al., 2007):

$$\Delta Q_G = c_p \frac{\Delta T_s}{\Delta t} \Delta z \tag{3}$$

where ΔT_s [K] is the difference in soil temperature T_s between two time steps of length Δt [s]; Δz [m] is the soil layer thickness between the plates and the surface; and c_p [J m^{-3} K^{-1}] is the specific heat of the soil, taken as:

$$c_p = c_{p,dry} + c_{p,water}\theta \quad (4)$$

where $c_{p,dry}$ and $c_{p,water}$ are values taken from the literature for a sandy loam and for water (1.28×10^6 and 4.184×10^6 J m^{-3} K^{-1}, respectively; Van Wijk, 1963) and θ [m^3 m^{-3}] is the volumetric water content of the soil.

Soil heat flux plates were subject to very frequent malfunctions. Fortunately, ΔQ_G measurements were almost continuous once on-site time series were merged, and correlation between soil heat flux plates measurements and ΔQ_G were high (R^2 between 0.7 and 0.9). Missing G values were obtained using a monthly linear regression with ΔQ_G.

To account for the measurement height of the eddy-covariance systems, storage fluxes of sensible heat and latent heat (ΔQ_H and $\Delta Q_{\lambda E}$) were also evaluated at each station using the method of Aubinet et al. (2001):

$$\Delta Q_H = \sum_{i=1}^{4} c_{p,i}\rho_i \frac{\Delta T_i}{\Delta t}\Delta z_i \quad (5)$$

$$\Delta Q_{\lambda E} = \sum_{i=1}^{4} L_{v,i}\rho_i \frac{\Delta q_i}{\Delta t}\Delta z_i \quad (6)$$

where subscript i applies to the four (one) measurement height for each variable of the Juvenile (Sapling) station; $\Delta T_a,i$ [K] and Δq_i [kg kg^{-1}] are the differences in T_a or q at height i between two time steps of length Δt [s]; and Δz_i [m] is the air layer thickness associated with each measurement probe. For the Juvenile station, Δz_i is 4.49 m, 3.74 m, 4.64 m and 1.50 m from bottom to top probe, respectively, while Δz is the measurement height (8.5 m) for the Sapling station.

Biomass heat storage (ΔQ_B) was computed for specific portion (upper and lower trunk, branches, needles or leaves) of each monitored tree using vegetation temperature measurements and the following general formula (Oliphant et al., 2004):

$$\Delta Q_{veg} = m_{veg} c_{p,veg} \frac{\Delta T_{veg}}{\Delta t} \quad (7)$$

where ΔQ_{veg} [W] is a heat storage within a specific tree portion; m_{veg} [kg] is its mass [kg]; $c_{p,veg}$ is its heat capacity [J kg^{-1} K^{-1}]; and ΔT_{veg} is the temperature variation during a time step of length Δt.

Specific properties of the trees were obtained from USDA (2007). Tree trunk portions were approximated as cylinders, and bulk temperature variations of the upper and lower trunks as a whole were calculated using the method outlined in Garai et al. (2010). Branch and needle temperatures were

taken as the average of branch thermistors. Branch mass was calculated using surveyed branch density with height and assuming that branch length decreases linearly from the bottom branches to the top of the tree. Needle mass was calculated using the empirical functions of Ter-Mikaelian & Korzukhin (1997). ΔQ_B was then taken as the sum of ΔQ_{veg} values from trunk, branch and needle for each tree species (the three balsam firs were averaged), and multiplied by species-specific stem densities surveyed around the flux tower (balsam fir: 0.26 m^{-2}; white spruce: 0.01 m^{-2}; white birch: 0.003 m^{-2}). Missing ΔQ_B values were filled with monthly linear regression with zero-set origin between heat storage and net radiation.

3. Comparison Sites

The energy budgets of the Montmorency Forest sites were compared to those of 15 sites located in the boreal forest that are described in Table 1. Data from European (BS1858, SP1907, SP1962) and United States (BS1945) sites were obtained from the Fluxnet 2015 dataset (available at: https://fluxnet.fluxdata.org), while data from Canadian sites were part of the FLUXNET Canada Research Network Canadian Carbon Program Data Collection, 1993-2014 (FLUXNET–Canada, 2016). Note that the Juvenile and Sapling sites are also featured in Table 1 as sites BF1993 and BF2003, respectively.

The sites used for comparisons are spread all across the circumpolar boreal biome and include most of the usual trees found in these regions at different stages of maturity. Annual averages of temperature are relatively constant throughout the sites, with variations between −2.0°C in Alaska (BS1945) and 3.9°C in Russia (BS1858). Climatological averages of annual cumulative precipitation vary greatly across sites, from the very dry Alaskan site (275 mm y^{-1}) to the humid sites of eastern Canada (MW1980 at 831 mm y^{-1}; BS1912, BS1975 and BS2000 at 961 mm y^{-1}), culminating at the main study sites in the Montmorency Forest receiving an average of 1583 mm y^{-1}.

Table 1 also presents the main references for each study site, in which instrumental setups are described. All sites featured standard eddy-covariance systems installed following diligent procedures. Data from the Fluxnet 2015 dataset was processed following methods outlined at https://fluxnet.fluxdata.org/data/fluxnet2015-dataset/data-processing/: every variable is rigorously quality-checked (Pastorello et al., 2014), meteorological variables are gap-filled using ERA-Interim reanalysis (Vuichard & Papale, 2015), while turbulent fluxes are gap-filled with the standard MDS procedure (Reichstein et al., 2005). FLUXNET–Canada (2016) dataset was processed following similar procedures described in Papale & Valentini (2003); Reichstein et al. (2005); Papale et al. (2006); Moffat et al. (2007).

In this study, we first present the fluxes that were uncorrected for energy balance closure (see section 5.1.1). To account for missing flux values at each site, we linearly scaled monthly sums of energy; multiplying the latter by the ratio of total number of periods in a given month over periods of

available data in the same month. Note that this procedure was also applied for annual sums of E and P.

This study also presents annual sums of E as components of the water budget at each site. However, every site experiences non-closure of the energy budget on a yearly basis (see section 5.1.1). Energy budget imbalance is a common problem with studies using eddy-covariance fluxes (*e.g.*, Baldocchi et al., 1997; Barr et al., 2001; 2006; Foken et al., 2010; Isabelle et al., 2018b), where the technique measures smaller turbulent fluxes ($H+ \lambda E$) than the available energy ($R_n - G - \Delta Q$). Probable causes behind this anomaly are well-described by Foken (2008), Leuning et al. (2012), and Stoy et al. (2013), among others. The consequence of this imbalance is that uncertainties are associated with E measurements, which are probably underestimated at all sites. For this reason, annual sums of E have to be corrected in water balance studies (Wohlfahrt et al., 2010).

In the present study, closure fraction (CF) was evaluated as the annual sums of turbulent fluxes ($H+ \lambda E$) divided by the annual sums of available energy ($R_n - G - \Delta Q$). However, precise and accurate measurements of G and ΔQ were not available at all sites: to be consistent for the sake of site comparison, we computed annual sums of available energy using only R_n. The relevance of this assumption is discussed in section 5.1.1. Annual E was then obtained by dividing measured annual E by annual CF, a method that preserves the Bowen ratio, *i.e.* the proportion of H to λE (Blanken et al., 1997; Twine et al., 2000; Wohlfahrt et al., 2010). This energy imbalance correction method was successfully applied in a hydrological study of the BOREAS region, in the Western Great Plains of Canada (Barr et al., 2012), and deemed appropriate to account for the underestimation of E in eddy-covariance measurements (Mauder et al., 2018).

Table 1: Description of the study sites. Site IDs are generated with main tree species at the site (first two letters) and approximate year of the last on-site disturbance, when vegetation started to grow back (last four numbers). LAI is the leaf area index at the start of the site study period, while GS is the average growing season length in days [d], calculated using the method of Bergeron et al. (2007). T_a and P are climatological averages of T_a and P on an annual basis. Age of tree stand is at the start of the site study period, described in the "Study years" column.

Site ID	Location	Coordinates	Altitude [m AMSL]	Vegetation (Age [y])	LAI [m^2 m^{-2}]	Study years	GS [d]	T_a [°C]	P [mm]	Reference
AS1928	Saskatchewan, Canada	53.63°N; 106.20°W	601	Aspen (70)	3.8	1997-2000; 2002-2010	227	0.4	467	Blanken et al. (1998)
BF1993	Québec, Canada	47.29°N; 71.17°W	855	Balsam Fir (25)	3.4	2016-2018	198	0.5	1583	Isabelle et al. (2018)
BF2003	Québec, Canada	47.29°N; 71.15°W	805	Balsam Fir (10)	2.9	2016-2018	199	0.5	1583	This study
BS1858	Fyodorovskoye, Russia	56.46°N; 32.92°E	265	Black Spruce (140)	3.5	1999-2012	268	3.9	711	Kurbatova et al. (2008)
BS1880	Saskatchewan, Canada	53.99°N; 105.11°W	629	Black Spruce (120)	5.6	2001-2010	216	0.4	467	Jarvis et al. (1997)
BS1912	Québec, Canada	49.69°N; 74.34°W	382	Black Spruce (95)	4.0	2005-2009	221	0.0	961	Bergeron et al. (2007)
BS1945	Alaska, USA	65.12°N; 147.49°W	210	Black Spruce (65)	0.7	2011-2012; 2014	173	-2.0	275	Ikawa et al. (2015)
BS1975	Québec, Canada	49.76°N; 74.57°W	385	Black Spruce (35)	3.5	2008-2010	233	0.0	961	Payeur-Poirier et al. (2012)
BS2000	Québec, Canada	49.27°N; 74.04°W	415	Black Spruce (5)	1.6	2005-2010	225	0.0	961	Giasson et al. (2006)
JP1915	Saskatchewan, Canada	53.92°N; 104.69°W	579	Jack Pine (90)	2.0	2004-2009	215	0.4	467	Baldocchi et al. (1997)
JP1975	Saskatchewan, Canada	53.88°N; 104.65°W	534	Jack Pine (30)	3.1	2005-2006	205	0.4	467	Mkhabela et al. (2009)
JP2002	Saskatchewan, Canada	53.94°N; 104.65°W	520	Jack Pine (5)	0.2	2005-2007	207	0.4	467	Mkhabela et al. (2009)
MW1930	Ontario, Canada	48.22°N; 82.16°W	340	Mixed Forest (75)	4.1	2006-2013	240	1.3	831	McCaughey et al. (2006)
SP1907	Sodankylä, Finland	67.36°N; 26.64°E	179	Scots Pine (110)	3.8	2003-2004	208	-0.4	527	Thum et al. (2007)
SP1962	Hyytiälä, Finland	61.85°N; 24.29°E	181	Scots Pine (35)	7.9	1997-2010	276	2.9	709	Suni et al. (2003)

4. Potential evapotranspiration calculation

This study focused on the effect of high precipitation on E, as it is viewed as a good proxy for water availability that can constrain land-atmosphere exchanges of water. However, to put comparison sites in perspective, it is also important to quantify site-specific values of the energy available for E and the potential water vapor content of the atmosphere. These concepts are well-described using potential evapotranspiration (E_p).

To evaluate E_p, we used the formula developed by Penman (1948). This equation was originally devised to quantify evaporation from an open-water surface, but it can also apply to saturated land surfaces. It combines energy-balance and mass-transfer approaches to evaluate E_p from available energy (R_n) and from atmospheric vapour deficit, which determines drying power of the air (ϕ). The equation goes as follows:

$$E_p = \frac{1}{\lambda}\left[\frac{\Delta_e}{(\Delta_e+\gamma)}R_n + \frac{\gamma}{(\Delta_e+\gamma)}\phi\right] \tag{8}$$

where E_p [kg m^{-2} s^{-1}] is the potential water vapor flux; λ [J kg^{-1}], the latent heat of vaporisation of water; Δ_e [Pa K^{-1}], the slope of saturation vapour pressure versus temperature curve; γ [Pa K^{-1}], the psychrometric constant; R_n [W m^{-2}], the net radiation; and ϕ [W m^{-2}], the drying power of the air defined by Katul & Parlange (1992) as:

$$\phi = \frac{c_p \kappa^2 \rho U D}{\gamma \ln\left(\frac{z_v - d_0}{z_{0v}}\right)\ln\left(\frac{z_m - d_0}{z_{0m}}\right)} \tag{9}$$

where c_p [J kg^{-1} K^{-1}] is the specific heat of the humid air; κ, the von Kármán constant (= 0.4); ρ [kg m^{-3}], the humid air density; U [m s^{-1}], the mean wind velocity measured at height z_m [m]; D [Pa], the vapor pressure deficit measured at height z_v [m]; γ [Pa K^{-1}], the psychrometric constant; z_{0m} and z_{0v} [m], the roughness lengths for momentum and humidity, respectively; d_0 [m], the zero-plane displacement height. d_0, z_{0m}, and z_{0v} are estimated with the site-specific mean vegetation height (h_v) (see Table 1) as $(2/3)h_v$, $0.1h_v$, and $0.01h_v$, respectively (Brutsaert, 1982; 2005).

Note that this evaluation of E_p is a theoretical upper bound: in reality, soil heat fluxes (G), and heat storage in biomass and air below measurement devices (ΔQ) should be subtracted from R_n to obtain available energy. Unfortunately, as was previously mentioned, these energy budget terms were not available at every comparison sites. To preserve consistency between measurement sites and be

consistent with E adjustments for closure fraction, we decided to compute E_p using only R_n, while noting that this probably results in an overestimation of E_p.

5. Results and Discussion

5.1. Comparison between boreal forest sites

5.1.1. Energy budget

Figure 2 presents annual cycles of monthly-averaged energy budget terms for each study site, for daytime periods only ($R_n > 0$), as it is when the majority of fluxes occur. Each plot includes one curve for each term per study year to outline interannual variability. Note that H and λE are here shown without energy imbalance correction. All study sites are characterized by classical net radiation curves culminating during (Northern Hemisphere) summer months, with obviously a very slight tendency towards higher values at southernmost latitudes (*e.g.*, SP1907 at 67.36°N has maximum $R_n \approx 400$ W m^{-2} vs. SP1962 at 61.85°N has maximum $R_n \approx 455$ W m^{-2}). All sites share similar annual trends: spring increases in R_n are counterbalanced by increasing H at first, but λE fluxes eventually rise around June when the growing season (and transpiration) blooms. The main difference between sites lies in the magnitude of summer λE peaks and the proportion of R_n they account for.

Two behaviours are exhibited in Figure 2: pine stands (JP1915, JP1975, JP2002, SP1907, and SP1962) and some black spruce stands (BS1858, BS1880, BS1912, and BS1945) see λE increasing in the summer without usually exceeding H, while other sites show a clear dominance of λE in the energy budget at the summer onset of transpiration. These discrepancies can stem from three plausible sources: (i) tree species; (ii) age of the tree stand; and (iii) meteorological conditions governing direct water and energy availability. The first two sources represent land surface conditions including soil type and moisture conditions.

Differences in energy budget across tree species are clear: stands including a large proportion of deciduous species (AS1928 and MW1930) exhibit a more pronounced summer peak in λE, the upward inflection point coinciding with leaf emergence. Balsam firs and black spruces usually thrive in wet environments and generate substantial λE given adequate water availability (McCaughey, 1978; Nijssen & Lettenmeier, 2002). On the contrary, pine stands grow in sandy well-drained soil and consequently produce lower λE fluxes (Nijssen & Lettenmeier, 2002; Mkhabela et al., 2009).

Pine stands appear to generate similar λE fluxes at different stages of maturity, as seen by comparing SP1907 with SP1962 or JP1915 with JP1975 and JP2002. The same can be said of balsam firs (BF1993 and BF2003), but black spruce stands from eastern Canada feature some differences. Indeed, the mature black spruces of BS1912 generate a notably lower summer peak of λE compared to

the juvenile stands of BS1975 or the saplings of BS2000. This behaviour is more thoroughly inspected in the next section.

All surveyed sites are subject to non-closure of the annual energy budget. Closure fraction (CF) varies between 0.50 and 0.99, while the interannual site averages vary between 0.69 (BS1945) and 0.90 (JP1915). Wherever the inclusion of other important energy budget terms such as G and/or ΔQ was possible, yearly values of CF did not improve much, with variations between -0.01 and 0.08 and an average variation of 0.01. For this reason, it seems that adjusting annual E values for energy budget closure using only R_n as available energy is a reasonable decision. It creates minimal uncertainties in yearly CF, and hence yearly E, and it is the most coherent procedure to apply to all sites.

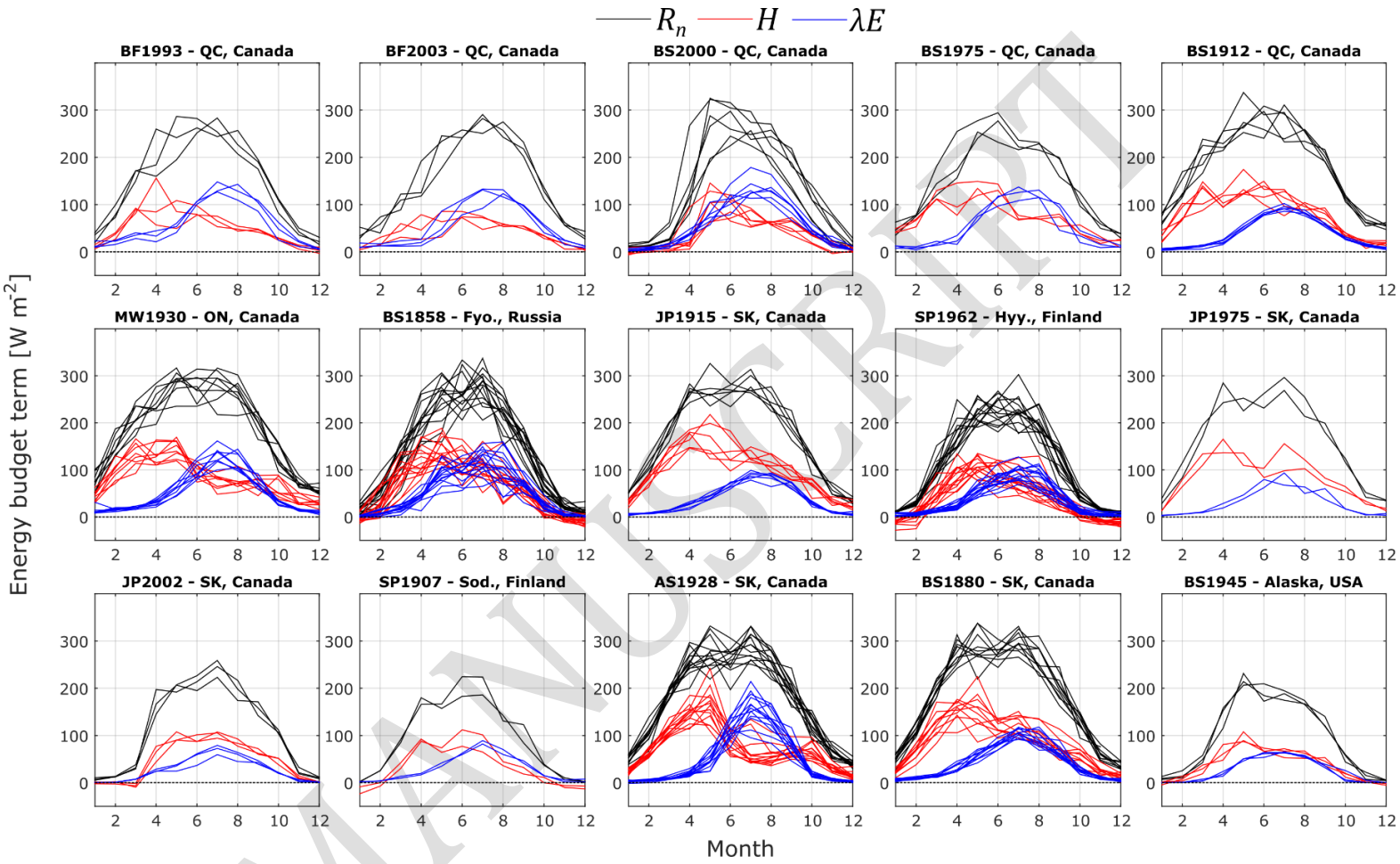

Figure 2: Annual cycles of monthly averaged net radiation (R_n, black lines) and sensible and latent heat fluxes (H and λE, uncorrected for energy imbalance, red and blue lines, respectively) for all study sites, including only daytime observations, defined as when $R_n > 0$). Each graph features one curve per study year for each variable. Sites are ordered by annual cumulative precipitation, from the site receiving most precipitation (BF1993) to the site receiving less (BS1945).

5.1.2. Evapotranspiration and precipitation

Yearly-scale variations of E and P as well as site-dependent evaporative demands (E_p) are outlined in Figure 3 and described in details in Table 2. All values of E are corrected for energy imbalance. These results bring forward the trends outlined in the previous section: sites with higher summer peaks of λE (AS1928, BF1993, BF2003, BS1975, BS2000, and MW1930) evidently are the sites enduring the strongest yearly E rates. The latter fluctuate amongst sites, from 194 mm y^{-1} for JP2002 to 446 mm y^{-1} at the Montmorency Forest juvenile balsam fir stand (BF1993).

Precipitation rates, as a proxy of water availability, appear very influential in the distribution of E rates, as can be seen in Table 2. Montmorency Forest sites (BF1993 and BF2003) clearly stand out as the sites receiving the most precipitation by a large margin, and consequently returning the greatest amount of water back to the atmosphere. In general, ranking sites by E rates or by P rates yields similar results, aside from some notable outliers. For example, AS1928 and BS1880 evaporate 422 and 383 mm y^{-1}; good for 7^{th} and 9^{th} rank by E, respectively, despite receiving the second and third lowest yearly precipitation. These sites are however characterized by strong energy inputs, as demonstrated by their very high E_p rates (2014 and 1806 mm y^{-1}, good for 2^{nd} and 5^{th} rank by E_p, respectively). Note that these findings stand with or without energy imbalance corrections. Such similarities between ranks are not visible when ranking sites by E and E_p, which seems to imply that boreal forest E strongly depends on water availability.

However, there is an intricate relationship between E, water availability (P) and evaporative demand (E_p). Figure 4 summarizes that relationship for each study site, that is: yearly-summed evaporative index (E/P) as a function of yearly-summed aridity index (E_p/P). The figure emulates the classical Budyko framework (Budyko, 1958, 1974), but note that this framework usually applies to climatologic rather than yearly averages (Gentine et al., 2012). The Montmorency Forest sites again stand out (blue circles and triangles): the sites have very low values of evaporative index and the lowest values of aridity index. Even if they generate the largest yearly evaporative rates, the important precipitation still outweighs evaporative losses by a lot. Recurring precipitation also decreases sun exposure and increase air humidity, which limits the potential to evaporate, indicating that water availability is rarely an issue.

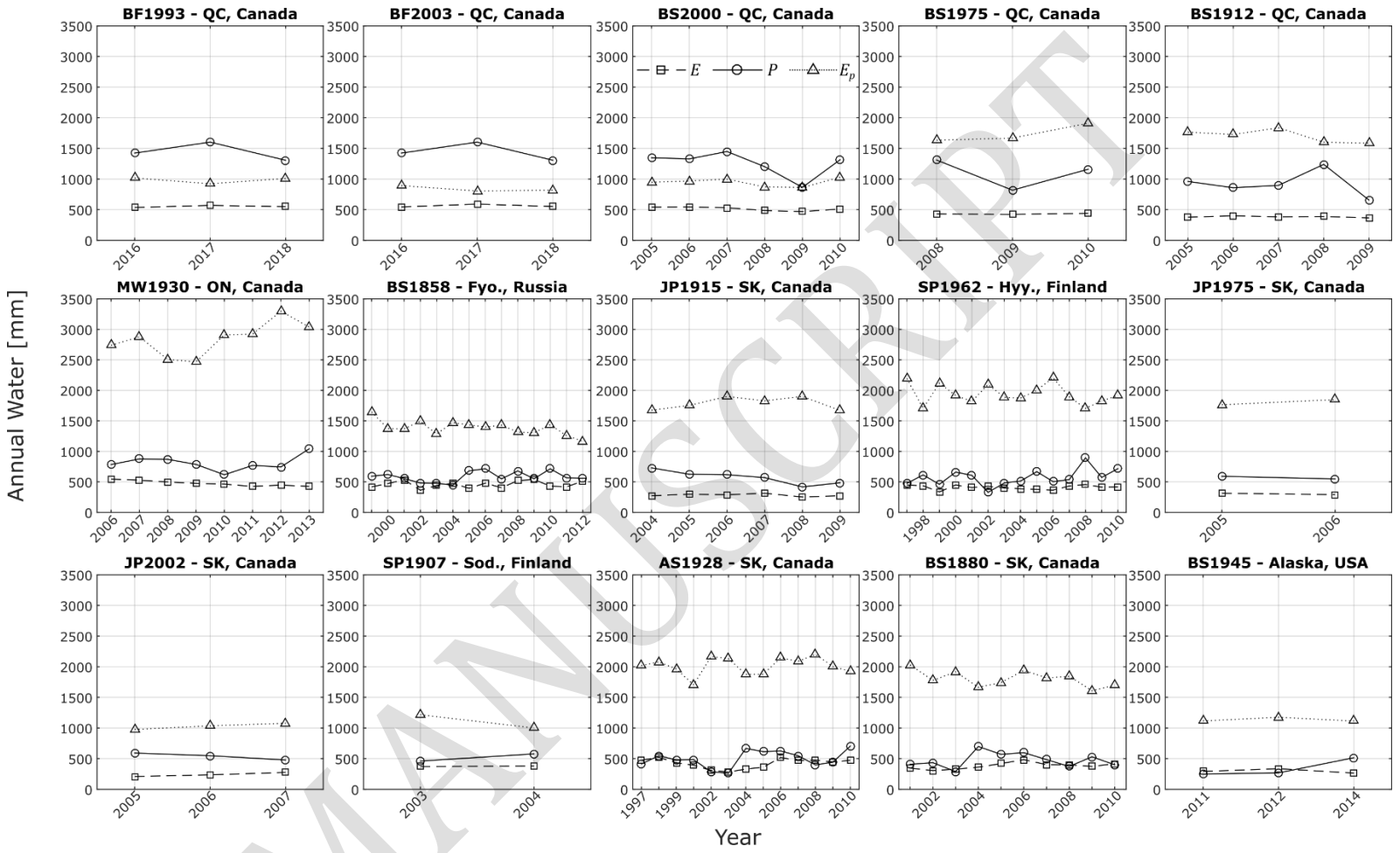

Figure 3: Interannual variations of annual cumulative precipitation P (full lines with circles), potential evapotranspiration E_p (dotted lines with triangles) and evapotranspiration E (dashed lines with squares) for each study site. Cumulatives are adjusted to account for missing values (see section 3). Sites are placed by annual precipitation rate ranking, from the site receiving most precipitation (BF1993) to the site receiving less precipitation (BS1945).

Table 2: Interannual averages ± standard deviations of *E, E** (uncorrected for energy imbalance), *P* and E_p for each study site, for the number of years in the second column. P_{clim} is the climatological average of precipitation (from Table 1). Sites are ordered by annual precipitation rate, from the site receiving the most precipitation (BF1993) to the site receiving the less precipitation (BS1945).

Site ID	# of years	P_{clim} [mm y^{-1}]	E [mm y^{-1}]	E^* [mm y^{-1}]	P [mm y^{-1}]	E_p [mm y^{-1}]
BF1993	3	1583	552 ± 17	446 ± 33	1444 ± 149	983 ± 52
BF2003	3	1583	562 ± 25	403 ± 55	1444 ± 149	839 ± 47
BS2000	6	961	514 ± 31	425 ± 40	1251 ± 205	946 ± 68
BS1975	3	961	431 ± 9	382 ± 9	1096 ± 252	1737 ± 151
BS1912	5	961	383 ± 12	286 ± 13	922 ± 211	1703 ± 108
MW1930	8	831	476 ± 45	380 ± 44	811 ± 123	2845 ± 274
BS1858	14	711	457 ± 55	353 ± 51	585 ± 87	1384 ± 117
JP1915	6	467	283 ± 22	253 ± 15	574 ± 110	1788 ± 105
SP1962	14	709	411 ± 35	300 ± 48	574 ± 137	1940 ± 163
JP1975	2	467	303 ± 16	218 ± 1	569 ± 31	1806 ± 59
JP2002	3	467	240 ± 33	194 ± 25	539 ± 57	1030 ± 51
SP1907	2	527	375 ± 5	276 ± 11	536 ± 52	1012 ± 102
AS1928	13	467	422 ± 79	370 ± 59	498 ± 138	2014 ± 142
BS1880	10	467	383 ± 52	311 ± 22	479 ± 116	1806 ± 126
BS1945	3	275	297 ± 36	202 ± 8	344 ± 149	1135 ± 36

Figure 4 displays an obvious trend amongst study sites: increasing the aridity index usually results in larger evaporative indexes, *i.e.*, the more arid the environment, the greater the proportion of *P* that is returned to the atmosphere. Note that the featured linear regression is statistically significant (p-value < 0.05). If we rearrange the linear regression equation, we obtain that $E = 0.12E_p + 0.31P$. This equation cannot be used single-handedly as a model for predicting annual *E*, but it outlines nicely the contribution from evaporative demand (E_p) and water availability (*P*) to *E* in boreal forests of the world. It also corroborates previous results that seem to point out to a slightly larger impact of water availability, or precipitation, to annual *E*. These trends are similarly visible when using *E* without energy imbalance corrections (not shown). Figure 4 also depicts the large interannual variability of most sites as well as uncertainty issues regarding the estimation of *E* and E_p, *e.g.*, E/P are above 1 in some situations.

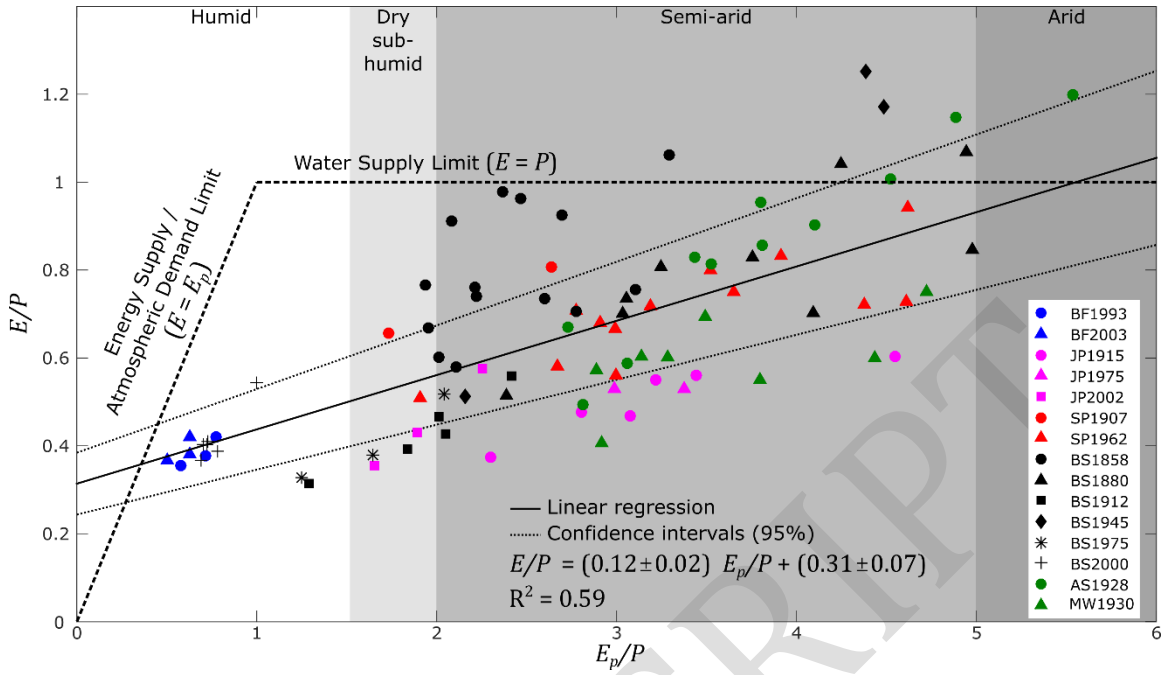

Figure 4: Evaporative index (evapotranspiration divided by precipitation E/P) vs. aridity index (potential evapotranspiration divided by precipitation E_p/P) for each study site. Each point represent one study year annual sums of E, P and E_p. Dashed lines show the demand limit (maximum possible E based on energy supply / atmospheric demand) and water supply limit (maximum E based on available water). Solid line is a least-squared linear regression with coefficients and R^2 introduced at the bottom of the graph, while dotted lines are the 95% confidence intervals lines corresponding to errors in linear regression coefficients.

We used multiple linear regressions to isolate the primary controls on annual evapotranspiration. The latter, for all sites and measurement years, was taken as the response variable, with predictors being annual precipitation (P [mm]), annual potential evapotranspiration (E_p [mm]), latitude (φ [°]), altitude (z [m]), and stand age (A [y]). The model took the following form:

$$E = 170\,\text{mm} + 0.21\,\frac{\text{mm}}{\text{mm}}\,P + 0.02\,\frac{\text{mm}}{\text{mm}}\,E_p + 0.73\,\frac{\text{mm}}{^\circ}\,\varphi - 0.04\,\frac{\text{mm}}{\text{m}}\,z + 0.49\,\frac{\text{mm}}{\text{y}}\,A \qquad (10)$$

and had an R^2 value of 0.40 while being statistically significant (p-value < 0.05). Interestingly, only P and A were significant contributors to the model (p-value < 0.05). These results highlight the high importance of annual precipitation on annual evapotranspiration. In addition, they identify stand age as an important predictor for annual E. Observations point towards minimal influences of latitude, altitude, and (more surprisingly) potential evapotranspiration. Latitude and annual precipitation are linked (R^2 = 0.37, p-value < 0.05) but not altitude and annual precipitation, primarily because all

Saskatchewan sites (AS1928, BS1880, JP1915, JP1975, and JP2002) have relatively high altitude (~565 m AMSL) and low precipitation.

The analysis was repeated species by species, whenever the number of data points allowed for it (*i.e.* not for balsam firs only and jack pines only; grouping aspens with mixed woods as "deciduous"; and grouping jack pines with scots pines as "pines"). Table 3 presents the coefficient of determination for each of these subset models, along with the associated p-values.

Table 3: Summary of multiple linear regressions results. Coefficient of determination R^2 are shown for models found for each groups of study sites. p-values indicate the significance level of each variables in the model: values in bold are significant at the 5% confidence level. Dashes indicate that the intercept value of the particular model was zero. Whenever a model has no significant contributing variable, the one with lowest p-value is in italics.

		p-value					
Groups	R^2	Intercept	P	E_p	φ	z	A
All	0.40	0.41	**0.00**	0.20	0.78	0.49	**0.01**
Deciduous	0.24	-	*0.18*	0.77	0.27	0.71	0.47
Conifers	0.53	0.72	**0.00**	0.43	0.29	0.21	**0.00**
Black Spruce	0.55	**0.00**	0.14	**0.00**	0.06	0.82	**0.00**
Scots Pine	0.32	-	0.54	*0.37*	0.96	0.75	0.52
Pines	0.85	0.55	*0.12*	0.34	0.80	0.22	0.58

These results show quite well that annual precipitation is commonly a driving factor in annual evapotranspiration, except maybe for Scots pines, which is mostly the SP1962 site. Stand age is the second most important variable: particularly for black spruces. Potential evapotranspiration is particularly influential for black spruces, and mildly for Scots pines and pines in general. Latitude and altitude again do not appear to be of influence.

As was described in section 4, E_p combines the effects of available energy, air humidity and atmospheric water vapor holding capacity to obtain maximum possible E. In Table 4, we quantify these effects by computing linear regressions between monthly summed E and monthly summed R_n or monthly averaged D (vapor pressure deficit) for all study site. Results show that R_n and D are important drivers of E: R_n explains between 60% and 89% of E variance, while D explains between 62% and 94% of E variance. All described linear regressions and correlations are statistically significant (p-value < 0.05), and these results are also observed with E uncorrected for energy imbalance (not shown). Similar results were obtained by Brümmer et al. (2012) for various Canadian sites (including AS1928, BS1880, BS1912, JP1915, and MW1930).

For most sites, correlation between E and D is close to or higher than correlation between E and R_n. BS1858 is the outlier, with R^2 values at 0.82 and 0.62 for linear regressions between E and R_n or D, respectively. Conifer-dominated sites in Saskatchewan exhibit smaller $E - D$ and $E - R_n$ slopes

than other sites, highlighting their tendency to limit *E* under low water availability conditions, even in times of high evaporative demand.

Table 4: Linear regression parameters (slope and intercept, with 95% confidence intervals) and coefficient of determination (R^2) between monthly summed *E* and: (i) monthly summed net radiation R_n; and (ii) monthly average 24-h vapour pressure deficit *D*.

Site ID	*E* vs. R_n			*E* vs. *D*		
	Slope [mm/(MJ m^{-2})]	Intercept [mm month^{-1}]	R^2	Slope [mm/Pa]	Intercept [mm month^{-1}]	R^2
AS1928	0.22 ± 0.03	0.30 ± 6.17	0.61	0.12 ± 0.01	-8.53 ± 6.37	0.66
BF1993	0.19 ± 0.05	13.46 ± 11.99	0.60	0.18 ± 0.04	8.32 ± 10.06	0.74
BF2003	0.25 ± 0.05	6.04 ± 9.85	0.77	0.19 ± 0.04	8.88 ± 10.57	0.72
BS1858	0.22 ± 0.02	1.16 ± 3.68	0.82	0.12 ± 0.01	4.58 ± 5.41	0.62
BS1880	0.15 ± 0.02	2.61 ± 4.41	0.72	0.09 ± 0.01	-0.03 ± 3.46	0.83
BS1912	0.16 ± 0.03	-0.16 ± 7.30	0.67	0.10 ± 0.01	2.50 ± 4.18	0.86
BS1945	0.15 ±0.02	5.04 ± 3.98	0.89	0.10 ± 0.01	-5.32 ± 5.39	0.87
BS1975	0.21 ± 0.04	-1.17 ± 9.61	0.74	0.13 ± 0.02	1.31 ± 7.39	0.82
BS2000	0.22 ± 0.02	8.43 ± 5.25	0.84	0.13 ± 0.01	0.40 ± 6.11	0.83
JP1915	0.12 ± 0.02	4.17 ± 4.48	0.66	0.07 ± 0.01	-0.51 ± 3.26	0.84
JP1975	0.15 ± 0.04	1.21 ± 8.28	0.75	0.08 ± 0.02	-2.90 ± 7.93	0.80
JP2002	0.13 ± 0.02	5.49 ± 3.19	0.87	0.06 ± 0.01	-1.64 ± 2.62	0.94
MW1930	0.20 ± 0.03	-0.90 ± 6.99	0.68	0.11 ± 0.01	0.29 ± 6.28	0.72
SP1907	0.18 ± 0.04	6.94 ± 8.74	0.77	0.13 ± 0.03	3.86 ± 8.00	0.82
SP1962	0.20 ± 0.01	5.09 ± 3.06	0.82	0.12 ± 0.01	1.08 ± 3.46	0.80

We must remind readers that E_p values calculated in this study are considered to be upper bounds, since the available energy used in the Penman formulation includes only R_n without *G* and ΔQ. However, as was seen in section 5.1.1, differences in available energy following the inclusion of *G* and/or ΔQ are fairly inconsequential on an annual basis. Plus, Penman E_p formulation in that form seems to include the proper drivers to describe *E* in the boreal forest, as *E* and E_p are highly correlated at all sites (R^2 between 0.50 and 0.89, average at 0.72).

This above analyses were performed using the simplest energy budget closure adjustment for *E*. Indeed, multiplying *E* by $1/CF$ preserves the Bowen ratio ($H/\lambda E$) for missing fluxes, but studies have demonstrated that this can induce an overcorrection (*e.g.*, Mauder et al., 2018). Nevertheless, such variation in the Bowen ratio are probably site-dependent, meaning that the attribution of site-specific

proportion of Bowen ratio for missing flux values could increase uncertainties in *E*. Note that all result-based conclusions in this section remain viable when using *E* uncorrected for energy imbalance.

Precipitation totals presented in this section are also tainted by probable uncertainties related to the common wind-induced undercatch problem, particularly with solid precipitation. However, these uncertainties depend on wind speed, and the latter does not vary much between sites (site-averaged wind speeds are between 1.72 and 3.48 m s^{-1}). Furthermore, differences in wind speed are more related to each site measurement height than actual differing wind regimes. Since every site team was aware of the undercatch problem, every instrument deployment was done following diligent procedures (shielded gauges installed at ground-level in wide forest clearings). Considering these precautions as well as likely similar uncertainties between sites, we believe our results still stand.

Despite the aforementioned limitations, this section has thoroughly demonstrated that the Montmorency Forest is receiving the highest cumulative precipitation of all surveyed sites, by a fair margin. But much higher *P* does not fully translate into much higher *E*. To put this in perspective, *E* values go from 240 mm y^{-1} (JP2002) to 562 mm y^{-1} (BF2003), an increase by a factor 2.34, while *P* values go from 344 mm y^{-1} (BS1945) to 1444 mm y^{-1} (BF1993, BF2003), an increase by a factor 4.20. It appears that *E* has a maximum value (or an upper physical limit), a result observed before in the boreal forest (Brümmer et al., 2012), but not necessarily elsewhere (Zhang et al., 1999). Reasons behind this behaviour could be physiological (ecosystem limit) and/or meteorological (*e.g.*, limited net radiation due to high cloud cover or/and an important atmospheric moisture convergence), but more studies are needed to elucidate this feature. Nevertheless, the Montmorency Forest stand-scale water budget definitely generates an excess of water that can substantially recharge groundwater storage or create strong runoffs.

5.2. Water allocation of a humid boreal forest

The Montmorency Forest sites are ideal to ascertain the effects of high annual precipitation on boreal forest water budgets. Figure 5 presents cumulative curves of every measured water budget components for catchment AB. *E* is a weighted combination of measurements at the Juvenile and Sapling flux towers ($E_{AB} = (A_A/A_{AB})E_{Juvenile} + (A_B/A_{AB})E_{Sapling}$), where A_A, A_B and A_{AB} are the areas of catchments A, B and AB, respectively). $E_{Juvenile}$ and $E_{Sapling}$ are corrected for non-closure of the energy budget, using *CF* calculated for the hydrological year (starting in October) and including measurements of *G* and ΔQ in the available energy estimation. Note that results from measurements taken for sub-catchment A only (not shown) are almost identical to those shown here.

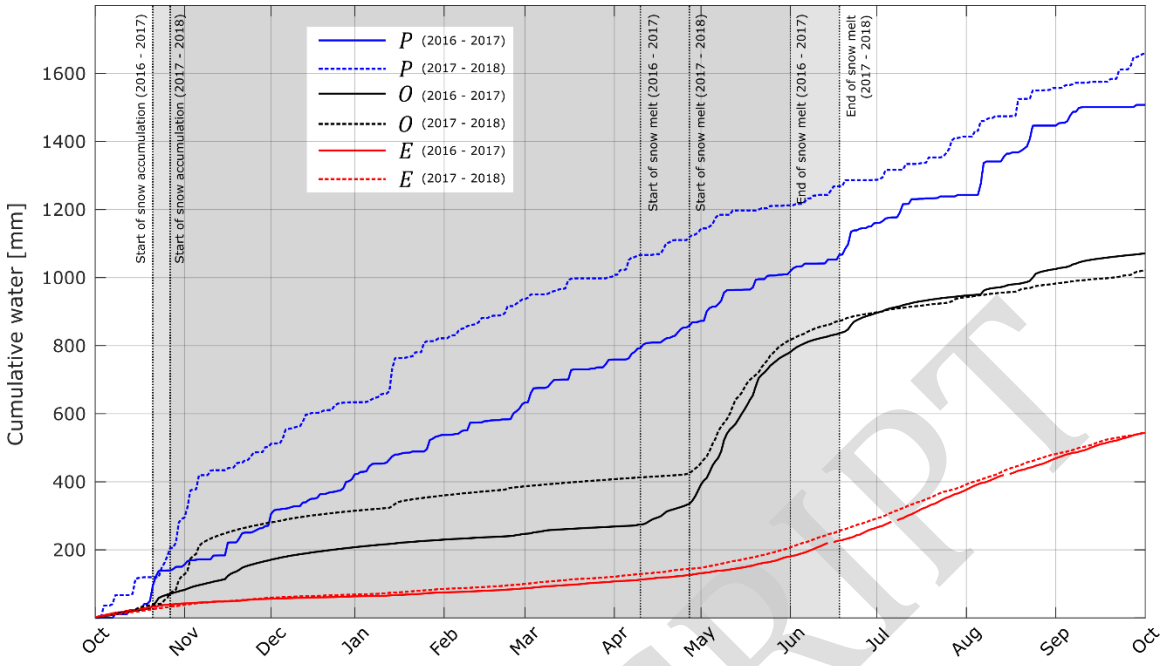

Figure 5: Cumulative precipitation *P* (blue), evapotranspiration *E* (red) and watershed outflow *O* (black) for hydrological years 2016-2017 (full lines) and 2017-2018 (dashed lines) for catchment AB. Hydrological years are defined from October 1 to September 30 to encompass winter snow-covered periods. The latter periods are illustrated using shades of grey on the graph.

As it is the case for most boreal watersheds, snow accumulation and melting are highly impactful on the Montmorency Forest water budget. During the two hydrological years of the study period, 44% and 33% of the annual precipitation fell in solid state, leading to a maximum seasonal snowpack depth of 213 cm and 180 cm for 2016-2017 and 2017-2018, respectively. Snowmelt generates a substantial proportion of annual watershed discharges: 503 mm and 456 mm, or 47% and 45% of total annual discharges in 2016-2017 and 2017-2018, respectively.

Throughout both years, *E* rates were maximized in summer, with 67% and 61% of annual *E* occurring from June to September inclusively in 2016-2017 and in 2017-2018, respectively. Instruments records show that 12% and 16% of annual *E* occurred as winter sublimation (when air temperature was below −2°C), in 2016-2017 and 2017-2018, respectively.

For both hydrological years, the water budget (Equation 2) did not fully close: subtracting annual *E* and *O* from annual *P* yielded residuals of −107 mm and 92 mm. These values correspond to 7% and 6% of annual precipitation for 2016-2017 and 2017-2018 respectively. Unfortunately, the ground water storage part of ΔS was not fully assessed. However, on a hydrological year time scale, storage variations in soil moisture and snowpack accumulation were not detected. Water table variations were not measured during the study period, but the small residuals in the water budget suggest that ground water storage may not vary much from the start of 2016 to the end of 2018.

Results need to be put in perspective by stating the uncertainties associated with each measured water budget term. Precipitation measurements are known to be subject to wind-induced undercatch (Kochendorfer et al., 2017). However, the Montmorency Forest is also a site dedicated to study these issues (*e.g.*, Pierre et al., 2019), and the use of DFIR data during winter minimizes uncertainties. Note that when DFIR measurements were available, measured precipitation at the MELCC station accounted for 79% of DFIR measurements, and annual precipitation height increased from 1383 to 1508 mm y^{-1} and from 1482 to 1659 mm y^{-1} for 2016-2017 and 2017-2018, respectively. Undercatch is also a problem with liquid precipitation, and can amount to 4-6% (Sevruk et al., 2009).

Errors on *O* are minimal, since rating curve for the weirs have been constructed and verified frequently over 50 years, and include ice-cover periods. Overflow events seldom happen but are accounted for in the rating curves. It is hypothesized that some water flows underground out of the (head) AB watershed, and piezometers have recently been installed to verify underground water movement and storage. *E* errors are estimated using the random uncertainty method (Finkelstein & Sims, 2001), and they amount to 18% of annual *E* for each hydrological year (*e.g.*, the variability in Figure 4). Uncertainties also stem from the assumption of spatial representativeness of the flux towers *E* and the surface-weighted combination method. Watershed *E* is frequently the greatest source of uncertainties in watershed modeling (Donohue et al., 2010; Seiller & Anctil, 2014).

Despite these uncertainties, results paint a clear picture of the watershed. As was concluded in previous studies (*e.g.*, Barr et al., 2012; Brümmer et al., 2012), *E* rates are capped between 500 and 600 mm y^{-1} even in the presence of high precipitation height and maximum water availability. Excess precipitation then necessarily generates runoff and streamflow or recharge of ground water, which is quite beneficial to the society. Water table recharge is plausible, considering that the immature canopy is unclosed, and hence water reaches and infiltrates the ground easily (Isabelle et al., 2018a). However, given the hilly topography of the site, subsurface flow to streams seems more probable. Nevertheless, it is clear that watershed discharge is the main water-evacuating process in place. This behaviour is typical for a mountainous headwater catchment.

6. Conclusion

The balsam fir – white birch stand of the Montmorency Forest vastly stands out as the area receiving the largest annual precipitation amongst all of the 15 studied boreal forested locations. All sites respond to increasing precipitation by generating more *E* fluxes, but dry environments tend to evaporate a larger proportion of annual precipitation because of higher evaporative demand. The Montmorency Forest thus provides supplemental information that complement the previously available (dryer) sites that were used in comparison. *E* appears to be capped at around 550 mm y^{-1}: this could be a physiological limit of boreal species and climate or because simultaneous increases in

P and E_p are unlikely given that precipitation imply cloud cover (hence reduced net radiation), which decreases E_p. More studies partitioning E in its main components (transpiration, ground evaporation, and evaporation of intercepted precipitation) are needed to further our understanding of this observed ecohydrological limit.

Using precise measurements of watershed discharges at the Montmorency Forest sites, this study also outlined the watershed-scale (3.6 km^2) water budget of two hydrological years in a high-precipitation balsam fir boreal forest. Since E appears to be bounded by a maximum annual value (≈30% of P), excess water mostly becomes water discharge. This behaviour is typical of water budgets of headwater mountainous catchments. Water table measurements are still needed to thoroughly describe the watershed regime, but results are upcoming on this front.

To conclude, this study offers a precise experimental description of the catchment hydrological regime of a humid boreal forest typical of northeastern North America. Given the probable climate-change induced increase in precipitation, our results should be taken in consideration by hydroclimate modellers, especially those focused in the boreal zones of the world. In particular, they should expect that increases in precipitation will generate more watershed outflows than evapotranspiration rises.

7. Acknowledgments

The authors acknowledge all Montmorency Forest staff, especially Patrick Pineault and Charles Villeneuve, for their extremely valuable help in the field. We also would like to thank Annie-Claude Parent, Dany Crépault, Denis Jobin, Jean-Pierre Tatchegnon Gbegan, Benjamin Bouchard, Sophie Robitaille, Derek Jensen, Chaoxun Hang, Pascale Girard, Martin Pharand, Gabriel Hould Gosselin, Fabien Gaillard Blancard, Marie-Hélène Asselin, Audrey Combes, Bram Hadiwijaya and Achut Parajuli for their help installing the Juvenile and Sapling towers and instrumentation. This work was supported by the Natural Sciences and Engineering Research Council of Canada (NSERC), Ouranos Consortium, Hydro-Québec, Environment and Climate Change Canada, and Ministère de l'Environnement et de la Lutte contre les Changements climatiques (MELCC), through NSERC project RDCPJ-477125-14, and by the the Fonds de recherche du Québec - Nature et Technologies (FRQNT).

This work used eddy covariance data acquired and shared by the FLUXNET community, including these networks: AmeriFlux, AfriFlux, AsiaFlux, CarboAfrica, CarboEuropeIP, CarboItaly, CarboMont, ChinaFlux, Fluxnet-Canada, GreenGrass, ICOS, KoFlux, LBA, NECC, OzFlux-TERN, TCOS-Siberia, and USCCC. The ERA-Interim reanalysis data are provided by ECMWF and processed by LSCE. The FLUXNET eddy covariance data processing and harmonization was carried out by the European Fluxes Database Cluster, AmeriFlux Management Project, and Fluxdata project of FLUXNET, with the support of CDIAC and ICOS Ecosystem Thematic Center, and the OzFlux, ChinaFlux and AsiaFlux offices.

8. References

Aubinet, M., Chermanne, B., Vandenhaute, M., Longdoz, B., Yernaux, M., & Laitat, E. (2001). Long term carbon dioxide exchange above a mixed forest in the Belgian Ardennes. *Agric. For. Meteorol.*, *108*, 293–315. doi:10.1016/ S0168-1923(01)00244-1.

Baldocchi, D. D., Vogel, C. A., & Hall, B. (1997). Seasonal variation of energy and water vapor exchange rates above and below a boreal jack pine forest canopy. *J. Geophys. Res. Atmos.*, *102*, 28939–28951. doi:10.1029/ 96JD03325.

Barber, V. A., Juday, G. P., & Finney, B. P. (2000). Reduced growth of Alaskan white spruce in the twentieth century from temperature-induced drought stress. *Nature*, *405*, 668. doi:10.1038/35015049.

Barr, A. G., Betts, A. K., Black, T. A., McCaughey, J., & Smith, C. (2001). Intercomparison of BOREAS northern and southern study area surface fluxes in 1994. *J. Geophys. Res. Atmos.*, *106*, 33543–33550. doi:10.1029/ 2001JD900070.

Barr, A., Griffs, T., Black, T. A., Lee, X., Staebler, R., Fuentes, J., Chen, Z., & Morgenstern, K. (2002). Comparing the carbon budgets of boreal and temperate deciduous forest stands. *Can. J. For. Res., 32*, 813–822. doi:10.1139/x01-131.

Barr, A., Morgenstern, K., Black, T. A., McCaughey, J., & Nesic, Z. (2006). Surface energy balance closure by the eddy-covariance method above three boreal forest stands and implications for the measurement of the CO2 flux. *Agric. For. Meteorol.*, *140*, 322–337. doi:10.1016/j.agrformet.2006.08.007.

Barr, A., Van der Kamp, G., Black, T. A., McCaughey, J., & Nesic, Z. (2012). Energy balance closure at the BERMS flux towers in relation to the water balance of the White Gull Creek watershed 1999–2009. *Agric. For. Meteorol.*, *153*, 3–13. doi:10.1016/j.agrformet.2011.05.017.

Bergeron, O., Margolis, H. A., Black, T. A., Coursolle, C., Dunn, A. L., Barr, A. G., & Wofsy, S. C. (2007). Comparison of carbon dioxide fluxes over three boreal black spruce forests in Canada. *Glob. Change Biol.*, *13*, 89–107. doi:10.1111/j.1365-2486.2006.01281.x.

Blanken, P., Black, T. A., Neumann, H., Den Hartog, G., Yang, P., Nesic, Z., Staebler, R., Chen, W., & Novak, M. (1998). Turbulent flux measurements above and below the overstory of a boreal aspen forest. *Boundary-Layer Meteorol.*, *89*, 109–140. doi:10.1023/A:1001557022310.

Blanken, P., Black, T. A., Yang, P., Neumann, H., Nesic, Z., Staebler, R., Den Hartog, G., Novak, M., & Lee, X. (1997). Energy balance and canopy conductance of a boreal aspen forest: partitioning overstory and understory components. *J. Geophys. Res. Atmos.*, *102*, 28915–28927. doi:10.1029/ 97JD00193.

Brandt, J., Flannigan, M., Maynard, D., Thompson, I., & Volney, W. (2013). An introduction to Canada's boreal zone: ecosystem processes, health, sustainability, and environmental issues. *Environ. Rev.*, *21*, 207–226. doi:10. 1139/er-2013-0040.

Brown, S., Petrone, R., Chasmer, L., Mendoza, C., Lazerjan, M., Landhäusser, S., Silins, U., Leach, J., & Devito, K. (2014). Atmospheric and soil moisture controls on evapotranspiration from above and within a Western Boreal Plain aspen forest. *Hydrol. Process., 28*, 4449–4462. doi:10.1002/hyp.9879.

Brümmer, C., Black, T. A., Jassal, R. S., Grant, N. J., Spittlehouse, D. L., Chen, B., Nesic, Z., Amiro, B. D., Arain, M. A., & Barr, A. G. (2012). How climate and vegetation type influence evapotranspiration and water use efficiency in Canadian forest, peatland and grassland ecosystems. *Agric. For. Meteorol.*, *153*, 14–30. doi:10.1016/j.agrformet.2011.04.008.

Brutsaert, W. (1982). *Evaporation into the Atmosphere: Theory, History, and Applications*. Reidel, Dordrecht, The Netherlands.

Brutsaert, W. (2005). *Hydrology: an Introduction*. Cambridge University Press, Cambridge, Mass.

Budyko, M. (1958). *The heat balance of the earth's surface*. Springer, Washington, DC.

Budyko, M. I. (1974). *Climate and life*. Academic, New York, NY.

Coursolle, C., Margolis, H. A., Barr, A. G., Black, T. A., Amiro, B. D., Mc-Caughey, J. H., Flanagan, L. B., Lafleur, P. M., Roulet, N. T., Bourque, C. P.-A. et al. (2006). Late-summer carbon fluxes from Canadian forests and peatlands along an east west continental transect. *Can. J. For. Res., 36*, 783–800. doi:10.1139/x05-270.

Donohue, R. J., McVicar, T. R., & Roderick, M. L. (2010). Assessing the ability of potential evaporation formulations to capture the dynamics in evaporative demand within a changing climate. *J. Hydrol.*, *386*, 186–197. doi:10.1016/j.jhydrol.2010.03.020.

D'Orangeville, L., Duchesne, L., Houle, D., Kneeshaw, D., Côté, B., & Pederson, N. (2016). Northeastern North America as a potential refugium for boreal forests in a warming climate. *Science*, *352*, 1452–1455. doi:10.1126/ science.aaf4951.

Finkelstein, P. L., & Sims, P. F. (2001). Sampling error in eddy correlation flux measurements. *J. Geophys. Res.*, *106*, 3503–3509. doi:10.1029/ 2000JD900731.

FLUXNET–Canada (2016). *FLUXNET Canada Research Network - Canadian Carbon Program Data Collection, 1993-2014*. ORNL DAAC, Oak Ridge, TN. doi:10.3334/ORNLDAAC/1335.

Foken, T. (2008). The energy balance closure problem: An overview. *Ecol. Appl.*, *18*, 1351–1367. doi:10.1890/06-0922.1.

Foken, T., Mauder, M., Liebethal, C., Wimmer, F., Beyrich, F., Leps, J.-P., Raasch, S., DeBruin, H. A. R., Meijninger, W. M. L., & Bange, J. (2010). Energy balance closure for the LITFASS-2003 experiment. *Theor. Appl. Climatol.*, *101*, 149–160.

Gao, Y., Markkanen, T., Aurela, M., Mammarella, I., Thum, T., Tsuruta, A., Yang, H., Aalto, T. et al. (2017). Response of water use efficiency to summer drought in a boreal Scots pine forest in Finland. *Biogeosciences, 14*, 4409–4422. doi:10.5194/bg-14-4409-2017.

Garai, A., Kleissl, J., & Smith, S. G. L. (2010). Estimation of biomass heat storage using thermal infrared imagery: application to a walnut orchard. *Boundary-Layer Meteorol., 137*, 333-342. doi:10.1007/s10546-010-9524-x.

Gauthier, S., Bernier, P., Kuuluvainen, T., Shvidenko, A., & Schepaschenko, D. (2015). Boreal forest health and global change. *Science*, *349*, 819–822. doi:10.1126/science.aaa9092.

Geissbühler, P., Siegwolf, R., & Eugster, W. (2000). Eddy covariance measurements on mountain slopes: the advantage of surface-normal sensor orientation over a vertical set-up. *Boundary-Layer Meteorol.*, *96*, 371–392. doi:10.1023/A:1002660521017.

Gentine, P., D'Odorico, P., Lintner, B. R., Sivandran, G., & Salvucci, G. (2012). Interdependence of climate, soil, and vegetation as constrained by the Budyko curve. *Geophys. Res. Lett.*, *39*. doi:10.1029/2012GL053492.

Giasson, M.-A., Coursolle, C., & Margolis, H. A. (2006). Ecosystem-level CO_2 fluxes from a boreal cutover in eastern Canada before and after scarification. *Agric. For. Meteorol.*, *140*, 23–40. doi:10.1016/j.agrformet.2006.08.001.

Goulden, M., Anderson, R., Bales, R., Kelly, A., Meadows, M., & Winston, G. (2012). Evapotranspiration along an elevation gradient in California's Sierra Nevada. *J. Geophys. Res. Biogeosci.*, *117*. doi:10.1029/2012JG002027.

Hammerle, A., Haslwanter, A., Schmitt, M., Bahn, M., Tappeiner, U., Cernusca, A., & Wohlfahrt, G. (2007). Eddy covariance measurements of carbon dioxide, latent and sensible energy fluxes above a meadow on a mountain slope. *Boundary-Layer Meteorol.*, *122*, 397–416. doi:10.1007/s10546-006-9109-x.

Hiller, R., Zeeman, M. J., & Eugster, W. (2008). Eddy-covariance flux measurements in the complex terrain of an alpine valley in Switzerland. *BoundaryLayer Meteorol.*, *127*, 449–467. doi:10.1007/s10546-008-9267-0.

Ikawa, H., Nakai, T., Busey, R. C., Kim, Y., Kobayashi, H., Nagai, S., Ueyama, M., Saito, K., Nagano, H., Suzuki, R. et al. (2015). Understory CO_2, sensible heat, and latent heat fluxes in a black spruce forest in interior Alaska. *Agric. For. Meteorol.*, *214*, 80–90. doi:10.1016/j.agrformet.2015.08.247.

Ilvesniemi, H., Pumpanen, J., Duursma, R., Hari, P., Keronen, P., Kolari, P., Kulmala, M., Mammarella, I., Nikinmaa, E., Rannik, Ü. et al. (2010). Water balance of a boreal Scots pine forest. *Boreal Environ. Res.*, *15*, 375–396.

IPCC (2013). Contribution of working group I to the fifth assessment report of the Intergovernmental Panel on Climate Change. In *Climate Change 2013: The Physical Science Basis*. Cambridge University Press, Cambridge, Mass.

Isabelle, P.-E., Nadeau, D. F., Asselin, M.-H., Harvey, R., Musselman, K. N., Rousseau, A. N., & Anctil, F. (2018a). Solar radiation transmittance of a boreal balsam fir canopy: Spatiotemporal variability and impacts on growing season hydrology. *Agric. For. Meteorol.*, *263*, 1–14. doi:10.1016/j.agrformet. 2018.07.022.

Isabelle, P.-E., Nadeau, D. F., Rousseau, A. N., & Anctil, F. (2018b). Water budget, performance of evapotranspiration formulations, and their impact on hydrological modeling of a small boreal peatland-dominated watershed. *Can. J. Earth Sci.*, *55*, 206–220. doi:10.1139/cjes-2017-0046.

Jarvis, P., Massheder, J., Hale, S., Moncrieff, J., Rayment, M., & Scott, S. (1997). Seasonal variation of carbon dioxide, water vapor, and energy exchanges of a boreal black spruce forest. *J. Geophys. Res. Atmos.*, *102*, 28953– 28966. doi:10.1029/97JD01176.

Katul, G. G., & Parlange, M. B. (1992). A Penman-Brutsaert model for wet surface evaporation. *Water Resour. Res.*, *28*, 121–126. doi:10.1029/91WR02324.

Kauppi, P. E., Posch, M., & Pirinen, P. (2014). Large impacts of climatic warming on growth of boreal forests since 1960. *PLoS One*, *9*, e111340. doi:10.1371/journal.pone.0111340.

Kochendorfer, J., Rasmussen, R., Wolff, M., Baker, B., Hall, M. E., Meyers, T., Landolt, S., Jachcik, A., Isaksen, K., Brækkan, R. et al. (2017). The quantification and correction of wind-induced precipitation measurement errors. *Hydrol. Earth Syst. Sci.*, *21*, 1973–1989. doi:10.5194/hess-21-1973-2017.

Kurbatova, J., Li, C., Varlagin, A., Xiao, X., & Vygodskaya, N. (2008). Modeling carbon dynamics in two adjacent spruce forests with different soil conditions in Russia. *Biogeosciences*, *5*, 969–980. doi:10.5194/bg-5-969-2008.

Landsberg, J. J., & Gower, S. T. (1997). *Applications of physiological ecology to forest management*. Academic Press, New York, NY.

Lavigne, M.-P. (2007). *Modélisation du régime hydrologique et de l'impact des coupes forestières sur l'écoulement du ruisseau des Eaux-Volées à l'aide d'HYDROTEL*. Master's thesis, Institut national de la recherche scientifique - Centre Eau Terre Environnement, Québec, Canada.

Leuning, R., Van Gorsel, E., Massman, W. J., & Isaac, P. R. (2012). Reflections on the surface energy imbalance problem. *Agric. For. Meteorol., 156*, 65-74. doi:10.1016/j.agrformet.2011.12.002.

Liu, P., Black, T. A., Jassal, R. S., Zha, T., Nesic, Z., Barr, A. G., Helgason, W. D., Jia, X., Tian, Y., Stephens, J. J. et al. (2019). Divergent long-term trends and interannual variation in ecosystem resource use efficiencies of a southern boreal old black spruce forest 1999–2017. *Glob. Change Biol.* doi:10.1111/gcb.14674.

Lloyd, A. H., & Bunn, A. G. (2007). Responses of the circumpolar boreal forest to 20th century climate variability. *Environ. Res. Lett.*, *2*, 045013. doi:10.1088/1748-9326/2/4/045013.

Mauder, M., & Foken, T. (2011). *Documentation and instruction manual of the eddy-covariance software package TK3*. Technical Report, Universität Bayreuth, Germany.

Mauder, M., Genzel, S., Fu, J., Kiese, R., Soltani, M., Steinbrecher, R., Zeeman, M., Banerjee, T., De Roo, F., & Kunstmann, H. (2018). Evaluation of energy balance closure adjustment methods by independent evapotranspiration estimates from lysimeters and hydrological simulations. *Hydrol. Process.*, *32*, 39–50. doi:10.1002/hyp.11397.

McCaughey, J. H. (1978). Energy balance and evapotranspiration estimates for a mature coniferous forest. *Can. J. For. Res., 8*(4), 456-462. doi:10.1139/x78-067.

McCaughey, J., Pejam, M., Arain, M., & Cameron, D. (2006). Carbon dioxide and energy fluxes from a boreal mixedwood forest ecosystem in Ontario, Canada. *Agric. For. Meteorol.*, *140*, 79–96. doi:10.1016/j.agrformet.2006. 08.010.

MELCC (2019). *Données du programme de surveillance du climat*. Direction générale de la surveillance du climat, Ministère de l'Environnement et de la Lutte contre les Changements Climatiques, Québec, Canada.

Mkhabela, M., Amiro, B., Barr, A., Black, T. A., Hawthorne, I., Kidston, J., McCaughey, J., Orchansky, A., Nesic, Z., Sass, A., Shashkov, A., & Zhab, T. (2009). Comparison of carbon dynamics and water use efficiency following fire and harvesting in Canadian boreal forests. *Agric. For. Meteorol.*, *149*, 783–794. doi:10.1016/j.agrformet.2008.10.025.

Moffat, A. M., Papale, D., Reichstein, M., Hollinger, D. Y., Richardson, A. D., Barr, A. G., Beckstein, C., Braswell, B. H., Churkina, G., & Desai, A. R. (2007). Comprehensive comparison of gap-filling techniques for eddy covariance net carbon fluxes. *Agric. For. Meteorol.*, *147*, 209–232.

Moncrieff, J., Clement, R., Finnigan, J., & Meyers, T. (2004). Averaging, detrending, and filtering of eddy covariance time series. In X. Lee, W. Massman, & B. Law (Eds.), *Handbook of micrometeorology: a guide for surface flux measurement and analysis* (pp. 7–31). Springer, Dordrecht, The Netherlands.

Moncrieff, J. B., Massheder, J., De Bruin, H., Elbers, J., Friborg, T., Heusinkveld, B., Kabat, P., Scott, S., Søgaard, H., & Verhoef, A. (1997). A system to measure surface fluxes of momentum, sensible heat, water vapour and carbon dioxide. *J. Hydrol.*, *188*, 589–611.

Nadeau, D. F., Pardyjak, E. R., Higgins, C. W., Huwald, H., & Parlange, M. B. (2013a). Flow during the evening transition over steep alpine slopes. *Q. J. R. Meteorol. Soc., 139*, 607-624. doi:10.1002/qj.1985.
Nadeau, D. F., Pardyjak, E. R., Higgins, C. W., & Parlange, M. B. (2013b). Similarity scaling over a steep alpine slope. *Boundary-Layer Meteorol.*, *147*, 401–419. doi:10.1007/s10546-012-9787-5.

Nijssen, B., & Lettenmaier, D. P. (2002). Water balance dynamics of a boreal forest watershed: White Gull Creek basin, 1994–1996. *Water Resour. Res.*, *38*. doi:10.1029/2001WR000699.

Nöel, P., Rousseau, A. N., Paniconi, C., & Nadeau, D. F. (2014). Algorithm for delineating and extracting hillslopes and hillslope width functions from gridded elevation data. *J. Hydrol. Eng.*, *19*, 366–374. doi:10.1061/(ASCE)HE.1943-5584.0000783.

Ochsner, T. E., Sauer, T. J., & Horton, R. (2007). Soil heat storage measurements in energy balance studies. *Agron. J.*, *99*, 311–319. doi:10.2134/ agronj2005.0103S.

Oldroyd, H. J., Pardyjak, E. R., Huwald, H., & Parlange, M. B. (2016). Adapting tilt corrections and the governing flow equations for steep, fully three-dimensional, mountainous terrain. *Boundary-Layer Meteorol.*, *159*, 539–565. doi:10.1007/s10546-015-0066-0.

Oliphant, A., Grimmond, C., Zutter, H., Schmid, H., Su, H.-B., Scott, S., Offerle, B., Randolph, J., & Ehman, J. (2004). Heat storage and energy balance fluxes for a temperate deciduous forest. *Agric. For. Meteorol., 126*, 185-201. doi:10.1016/j.agrformet.2004.07.003.

Oltchev, A., Cermak, J., Gurtz, J., Tishenko, A., Kiely, G., Nadezhdina, N., Zappa, M., Lebedeva, N., Vitvar, T., Albertson, J. et al. (2002). The response of the water fluxes of the boreal forest region at the Volga's source area to climatic and land-use changes. *Phys. Chem. Earth Pt A/B/C*, *27*, 675–690. doi:10.1016/S1474-7065(02)00052-9.

Ono, K., Mano, M., Miyata, A., & Inoue, Y. (2008). Applicability of the planar fit technique in estimating surface fluxes over flat terrain using eddy covariance. *J. Agric. Meteorol. (Jpn)*, *64*, 121–130.

Pan, Y., Birdsey, R. A., Fang, J., Houghton, R., Kauppi, P. E., Kurz, W. A., Phillips, O. L., Shvidenko, A., Lewis, S. L., Canadell, J. G., Ciais, P., Jackson, R. B., Pacala, S., McGuire, A. D., Piao, S., Rautiainen, A., Sitch, S., & Hayes, D. (2011). A large and persistent carbon sink in the world's forests. *Science*, *333*, 988–993. doi:10.1126/science.1201609.

Papale, D., Reichstein, M., Aubinet, M., Canfora, E., Bernhofer, C., Kutsch, W., Longdoz, B., Rambal, S., Valentini, R., Vesala, T. et al. (2006). Towards a standardized processing of Net Ecosystem Exchange measured with eddy covariance technique: algorithms and uncertainty estimation. *Biogeosciences*, *3*, 571–583.

Papale, D., & Valentini, R. (2003). A new assessment of European forests carbon exchanges by eddy fluxes and artificial neural network spatialization. *Glob. Change Biol.*, *9*, 525–535. doi:10.1046/j.1365-2486.2003.00609.x.

Pastorello, G., Agarwal, D., Papale, D., Samak, T., Trotta, C., Ribeca, A., Poindexter, C., Faybishenko, B., Gunter, D., Hollowgrass, R. et al. (2014). Observational data patterns for time series data quality assessment. In *2014 IEEE 10th International Conference on e-Science* (pp. 271–278). IEEE volume 1.

Payeur-Poirier, J.-L., Coursolle, C., Margolis, H. A., & Giasson, M.-A. (2012). CO_2 fluxes of a boreal black spruce chronosequence in eastern North America. *Agric. For. Meteorol.*, *153*, 94–105. doi:10.1016/j.agrformet.2011.07.009.

Penman, H. L. (1948). Natural evaporation from open water, bare soil and grass. *Proc. R. Soc. Lond.*, *A193*, 120–145.

Pierre, A., Jutras, S., Smith, C., Kochendorfer, J., Fortin, V., & Anctil, F. (2019). Evaluation of catch efficiency transfer functions for unshielded and single-Alter-shielded solid precipitation measurements. *J. Atmos. Ocean. Tech*. doi:10.1175/JTECH-D-18-0112.1.

Reichstein, M., Falge, E., Baldocchi, D., Papale, D., Aubinet, M., Berbigier, P., Bernhofer, C., Buchmann, N., Gilmanov, T., & Granier, A. (2005). On the separation of net ecosystem exchange into assimilation and ecosystem respiration: review and improved algorithm. *Glob. Change Biol.*, *11*, 1424– 1439. doi:10.1111/j.1365-2486.2005.001002.x.

Saugier, B., Granier, A., Pontailler, J., Dufrene, E., & Baldocchi, D. (1997). Transpiration of a boreal pine forest measured by branch bag, sap flow and micrometeorological methods. *Tree Physiol.*, *17*, 511–519. doi:10.1093/ treephys/17.8-9.511.

Schaphoff, S., Reyer, C. P., Schepaschenko, D., Gerten, D., & Shvidenko, A. (2016). Tamm Review: Observed and projected climate change impacts on Russia's forests and its carbon balance. *Forest Ecol. Manag.*, *361*, 432–444. doi:10.1016/j.foreco.2015.11.043.

Seiller, G., & Anctil, F. (2014). Climate change impacts on the hydrologic regime of a Canadian river: comparing uncertainties arising from climate natural variability and lumped hydrological model structures. *Hydrol. Earth Syst. Sci.*, *18*, 2033–2047. doi:10.5194/hess-18-2033-2014.

Sellers, P., Hall, F., Margolis, H., Kelly, B., Baldocchi, D., den Hartog, G., Cihlar, J., Ryan, M. G., Goodison, B., Crill, P. et al. (1995). The Boreal Ecosystem–Atmosphere Study (BOREAS): an overview and early results from the 1994 field year. *Bull. Am. Meteorol. Soc.*, *76*, 1549–1577. doi:10.1175/1520-0477(1995)076<1549:TBESAO>2.0.CO;2.

Sellers, P. J., Hall, F. G., Kelly, R. D., Black, T. A., Baldocchi, D., Berry, J., Ryan, M., Ranson, K. J., Crill, P. M., Lettenmaier, D. P. et al. (1997). BOREAS in 1997: Experiment overview, scientific results, and future directions. *J. Geophys. Res. Atmos.*, *102*, 28731–28769. doi:10.1029/97JD03300.

Serrano-Ortiz, P., Sánchez-Cañete, E., Olmo, F., Metzger, S., Pérez-Priego, O., Carrara, A., Alados-Arboledas, L., & Kowalski, A. (2016). Surface-parallel sensor orientation for assessing energy balance components on mountain slopes. *Boundary-Layer Meteorol., 158*, 489-499. doi:10.1007/s10546-015-0099-4.

Sevruk, B., Ondras, M., & Chvíla, B. (2009). The WMO precipitation measurement intercomparisons. *Atmos. Res.*, *92*, 376–380. doi:10.1016/j.atmosres. 2009.01.016.

Stiperski, I., & Rotach, M. W. (2016). On the measurement of turbulence over complex mountainous terrain. *Boundary-Layer Meteorol.*, *159*, 97–121. doi:10.1007/s10546-015-0103-z.

Stoy, P. C., Mauder, M., Foken, T., Marcolla, B., Boegh, E., Ibrom, A., Arain, M.A., Arneth, A., Aurela, M., Bernhofer, C. & Cescatti, A., (2013). A data-driven analysis of energy balance closure across FLUXNET research sites: The role of landscape scale heterogeneity. *Agric. For. Meteorol., 171*, 137-152. doi:10.1016/j.agrformet.2012.11.004.

Suni, T., Rinne, J., Reissell, A., Altimir, N., Keronen, P., Rannik, U., Maso, M., Kulmala, M., & Vesala, T. (2003). Long-term measurements of surface fluxes above a Scots pine forest in Hyytiälä, southern Finland, 1996-2001. *Boreal Environ. Res.*, *8*, 287–302.

Ter-Mikaelian, M. T., & Korzukhin, M. D. (1997). Biomass equations for sixty-five North American tree species. *For. Ecol. Manage., 97*, 1-24. doi:10.1016/S0378-1127(97)00019-4.

Thum, T., Aalto, T., Laurila, T., Aurela, M., Kolari, P., & Hari, P. (2007). Parametrization of two photosynthesis models at the canopy scale in a northern boreal Scots pine forest. *Tellus B*, *59*, 874–890. doi:10.1111/j.1600-0889.2007.00305.x.

Tremblay, Y., Rousseau, A. N., Plamondon, A. P., Levesque, D., & Jutras, S. (2008). Rainfall peak flow response to clearcutting 50% of three small watersheds in a boreal forest, Montmorency Forest, Quebec. *J. Hydrol.*, *352*, 67–76.

Tremblay, Y., Rousseau, A. N., Plamondon, A. P., Lévesque, D., & Prévost, M. (2009). Changes in stream water quality due to logging of the boreal forest in the Montmorency Forest, Quebec. *Hydrol. Process.*, *23*, 764–776. doi:10.1002/hyp.7175.

Turnipseed, A., Blanken, P., Anderson, D., & Monson, R. K. (2002). Energy budget above a high-elevation subalpine forest in complex topography. *Agric. For. Meteorol.*, *110*, 177–201. doi:10.1016/S0168-1923(01)00290-8.

Twine, T. E., Kustas, W., Norman, J., Cook, D., Houser, P., Meyers, T., Prueger, J., Starks, P., & Wesely, M. (2000). Correcting eddy-covariance flux underestimates over a grassland. *Agric. For. Meteorol.*, *103*, 279–300. doi:10.1016/S0168-1923(00)00123-4.

USDA (2007). *The Encyclopedia of Wood*. U.S. Department of Agriculture, Skyhorse Publishing Inc. New York, NY.

Van Wijk, W. (1963). *Physics of Plant Environment*. North Holland Publishing Co., Amsterdam, Denmark.

Vickers, D., & Mahrt, L. (1997). Quality control and flux sampling problems for tower and aircraft data. *J. Atmos. Ocean. Tech.*, *14*, 512–526.

Vuichard, N., & Papale, D. (2015). Filling the gaps in meteorological continuous data measured at FLUXNET sites with ERA-Interim reanalysis. *Earth Syst. Sci. Dat.*, *7*, 157–171. doi:10.5194/essd-7-157-2015.

Walker, X. J., Mack, M. C., & Johnstone, J. F. (2015). Stable carbon isotope analysis reveals widespread drought stress in boreal black spruce forests. *Glob. Change Biol.*, *21*, 3102–3113. doi:10.1111/gcb.12893.

Webb, E. K., Pearman, G. I., & Leuning, R. (1980). Correction of flux measurements for density effects due to heat and water vapour transfer. *Q. J. R. Meteorol. Soc.*, *106*, 85–100.
Whiteman, C. D., & Allwine, K. J. (1986). Extraterrestrial solar radiation on inclined surfaces. *Environ. Soft.*, *1*, 164–169.

Wilczak, J. M., Oncley, S. P., & Stage, S. A. (2001). Sonic anemometer tilt correction algorithms. *Boundary-Layer Meteorol.*, *99*, 127–150. doi:10.1023/ A:1018966204465.

Wohlfahrt, G., Irschick, C., Thalinger, B., Hörtnagl, L., Obojes, N., & Hammerle, A. (2010). Insights from independent evapotranspiration estimates for closing the energy balance: a grassland case study. *Vadose Zone J.*, *9*, 1025–1033. doi:10.2136/vzj2009.0158.

Yang, D. (2014). Double fence intercomparison reference (DFIR) vs. bush gauge for “true” snowfall measurement. *J. Hydrol.*, *509*, 94–100. doi:10.1016/j. jhydrol.2013.08.052.

Zha, T., Barr, A. G., van der Kamp, G., Black, T. A., McCaughey, J. H., & Flanagan, L. B. (2010). Interannual variation of evapotranspiration from forest and grassland ecosystems in western Canada in relation to drought. *Agric. For. Meteorol., 150*, 1476–1484. doi:10.1016/j.agrformet.2010.08.003.

Zhang, L., Walker, G. R., & Dawes, W. (1999). *Predicting the effect of vegetation changes on catchment average water balance*. Technical Report 99/12 Cooperative Research Center for Catchment Hydrology, CSIRO Land and Water, Canberra, Australia.